








Quantum and classical spin dynamics across temperature scales in the $S = 1/2$ Heisenberg antiferromagnet

Pyeongjae Park ^{1,*}, G. Sala,² Daniel M. Pajerowski ³, Andrew F. May ¹, James A. Kolopus,¹ D. Dahlbom ³,
Matthew B. Stone ^{3,†}, Gábor B. Halász ^{1,‡} and Andrew D. Christianson ^{1,§}

¹Materials Science & Technology Division, Oak Ridge National Laboratory, Oak Ridge, Tennessee 37831, USA

²Oak Ridge National Laboratory, Oak Ridge, Tennessee 37831, USA

³Neutron Scattering Division, Oak Ridge National Laboratory, Oak Ridge, Tennessee 37831, USA



(Received 14 May 2024; accepted 25 July 2024; published 19 August 2024)

Using the framework of semiclassical Landau-Lifshitz dynamics (LLD), we conduct a systematic investigation of the temperature-dependent spin dynamics in the $S = 1/2$ Heisenberg square-lattice antiferromagnet (SAFM). By performing inelastic neutron scattering measurements on $\text{Zn}_2\text{VO}(\text{PO}_4)_2$ (ZVPO) and corresponding finite-temperature spin dynamics simulations based on LLD, we present a comprehensive analysis that bridges quantum and classical spin dynamics over a broad temperature range. First, remarkable agreement between experimental data and LLD simulations is found in the paramagnetic phase of ZVPO, demonstrating the capability of LLD in accurately determining the spin Hamiltonian of $S = 1/2$ systems and capturing the quantum-to-classical crossover of their spin dynamics. Second, by analyzing the discrepancies between the experimental data and the LLD simulations at lower temperatures, we determine the experimental temperature dependence of the quantum effects in the excitation spectrum of the $S = 1/2$ SAFM: the quantum renormalization factor for the magnon energies and the quantum continuum above the one-magnon bands. Notably, the emergence of each quantum effect is found to correlate with the formation of three-dimensional long-range order. This work demonstrates the utility of LLD in gaining experimental insights into the temperature-induced modifications of quantum spin dynamics and their convergence towards classical expectations at higher temperatures. This motivates further applications to more challenging quantum antiferromagnets dominated by stronger quantum fluctuations.

DOI: [10.1103/PhysRevResearch.6.033184](https://doi.org/10.1103/PhysRevResearch.6.033184)

Understanding the collective phenomena of quantum antiferromagnets remains an ongoing challenge, especially in low-dimensional systems where quantum fluctuations are enhanced relative to three-dimensional antiferromagnets. Recent inelastic neutron scattering (INS) studies on various two-dimensional (2D) $S = 1/2$ antiferromagnets have unveiled a plethora of quantum phenomena which illustrate deviations from classical spin dynamics. These deviations include the significant renormalization of magnon energies [1–4], pronounced magnon decay [5,6], a highly structured multimagnon continuum [5,7], and most interestingly the emergence of fractionalized excitations [2,8–12]. While these phenomena highlight the diverse landscape of quantum magnetism, they also introduce hurdles in modeling the excitation spectra with traditional semiclassical methods, such as

linear spin-wave theory (LSWT), which are typically used to deduce spin Hamiltonians. Thus, the accurate identification of the spin Hamiltonian in a quantum antiferromagnet frequently calls for either sophisticated quantum spin dynamics calculations [7,13,14] or artificially suppressing inherent quantum fluctuations by, for example, applying a strong external magnetic field [7,15,16]. Notably, both approaches require considerable theoretical and/or experimental effort.

Introducing thermal fluctuations by increasing the temperature, a cornerstone variable in condensed-matter physics, can significantly aid in exploring the spin dynamics of quantum antiferromagnets. Raising the temperature moves quantum magnets into a regime where thermal fluctuations begin to dominate quantum fluctuations, which enables the following two investigative approaches. First, for temperatures T substantially exceeding the magnetic energy scale, one can determine the spin Hamiltonian using straightforward semiclassical spin dynamics theories. Second, and perhaps more intriguingly, one can then track deviations from semiclassical spin dynamics as T decreases towards the magnetic energy scale, which reveals how quantum fluctuations begin to impact the behavior of the system. Such a quantum-to-classical crossover can potentially deepen our understanding of the collective quantum phenomena found in $S = 1/2$ antiferromagnets. This approach, however, requires a simulation technique that systematically incorporates thermal

*Contact author: parkp@ornl.gov

†Contact author: stonemb@ornl.gov

‡Contact author: halaszg@ornl.gov

§Contact author: christiansad@ornl.gov

fluctuations into spin dynamics, which has been deemed challenging [17].

Recent studies have made substantial progress in addressing the aforementioned technical challenge using a range of methodologies [17–19]. In particular, employing Landau-Lifshitz dynamics (LLD) to numerically calculate dynamical spin-spin correlations via the time evolution of real-space spin configurations emerges as especially promising [20,21]. The primary benefit of this approach lies in its ability to provide an energy-resolved profile of spin dynamics at finite temperatures. This allows for the fitting of multidimensional dynamical structure factors $S(\mathbf{q}, \omega)$, which, due to the rich information available across both momentum and energy dimensions, facilitates the determination of the spin Hamiltonian with high fidelity, despite the typically broad and diffuse spectra found at high temperatures [6,11]. Moreover, the recent introduction of a temperature-dependent renormalization technique associated with the size of magnetic moments [17] has vastly extended the temperature range over which the LLD approach can accurately capture the energy scale of magnetic excitations (see the Supplemental Material for further explanation [22]). While these features make LLD a promising approach for modeling spin dynamics under sizable thermal fluctuations, its predictions for $S = 1/2$ quantum antiferromagnets have not yet been comprehensively compared with temperature-dependent experimental data. In contrast, for classical systems with larger S values ($S > 1/2$), the interplay between thermal fluctuations and spin dynamics has been investigated by several studies [17,25,26].

The $S = 1/2$ Heisenberg square-lattice antiferromagnet (SAFM) stands out as an ideal system for assessing the capabilities and limitations of LLD in describing the spin dynamics of quantum antiferromagnets under sizable thermal fluctuations. This is because the quantum effects observed in its excitation spectrum are well established by extensive previous studies [4,8,9,27–29] and are less complex than those in other lattice geometries [2,5]. Key quantum phenomena in the $S = 1/2$ SAFM include (i) a momentum-independent spin-wave energy enhancement due to an overall quantum renormalization factor Z_c [4,30,31], (ii) a two-magnon continuum above the one-magnon modes [4,9,32,33], and (iii) downward renormalization along with continuum scattering around $\mathbf{q} = (\pi, 0)$ attributed to fractionalized quasiparticles [8,9]. Despite these features, the overall magnetic excitation spectrum remains similar to classical spin dynamics predictions. Hence, a comparative analysis with LLD simulations, even though discrepancies are anticipated at low temperatures, can yield insightful conclusions.

This work presents a successful application of the semiclassical LLD approach to elucidate the temperature-driven evolution of quantum spin dynamics in the $S = 1/2$ Heisenberg SAFM. By conducting INS measurements of the $S = 1/2$ Heisenberg SAFM $\text{Zn}_2\text{VO}(\text{PO}_4)_2$ (ZVPO) and corresponding finite-temperature spin dynamics simulations through a standardized protocol proposed in this study, we engage in a thorough comparison of quantum versus classical spin dynamics over a broad temperature range $0.5T_N < T < 21.3T_N$, with T_N the Néel temperature. At temperatures well above $5T_N$, LLD simulations correspond remarkably well with experimental observations and yield reliable determination of

exchange parameters. Notably, this agreement persists down to approximately $1.1T_N$ upon incorporating an additional scale factor for the excitation energies to account for the quantum renormalization factor Z_c not included in the LLD simulation. Moreover, by analyzing the discrepancy between measured spectra and LLD simulations at lower temperatures, we delve into how thermal fluctuations dissipate quantum effects within the excitation spectrum of the $S = 1/2$ SAFM. The discussion extends to potential applications for other quantum magnetic systems and possible future improvements to the current LLD framework.

The synthesis and characterization methods of polycrystalline ZVPO are provided in the Supplemental Material [22]. The INS data were collected with 9.3 g of powder ZVPO at the Cold Neutron Chopper Spectrometer (CNCS) at the Spallation Neutron Source, using incident neutron energies of 3.32 and 1.55 meV. Data were collected at 23 different temperatures between 1.9 K (base) and 80 K under standard high-flux chopper conditions. No background subtraction was performed on the data presented in this work. Instead, a constant background was estimated during the comparative analysis with the calculated magnetic excitation spectra for $T \gg T_N$ (see the Supplemental Material [22]). The energy- and momentum-resolved dynamical susceptibility $\chi''(\mathbf{q}, E)$ was calculated from the time evolution of the spin system simulated by LLD, using the SU(N)NY package [20,34]. A detailed step-by-step protocol for this calculation is described in the Supplemental Material [22]. Instrumental energy and momentum resolutions for the simulation were estimated using the PYCHOP package in MANTID [35] and the full width at half maximum of the (100) magnetic Bragg peak of ZVPO along the $|\mathbf{q}|$ axis, respectively.

ZVPO is a nearly ideal realization of the $S = 1/2$ Heisenberg SAFM (Fig. 1). Previous bulk characterizations and powder neutron diffraction studies have identified the onset of long-range order below the Néel temperature $T_N = 3.75$ K [36–38]. Neutron diffraction data further revealed a Néel-type spin configuration for each V^{4+} square-lattice layer, with interlayer alignment being ferromagnetic [see Fig. 1(b)] [36]. The magnetic moments of V^{4+} ions are oriented along the c axis. The elastic component (-0.1 meV $< E < 0.1$ meV for $E_i = 3.32$ meV neutrons) of our powder INS data reveals a (100) magnetic Bragg peak for $T < 3.8$ K [Fig. 1(d)], consistent with previous studies [36].

The magnetism of ZVPO can be described by the minimal spin model

$$\hat{H} = J_1 \sum_{(i,j)_1} \hat{\mathbf{S}}_i \cdot \hat{\mathbf{S}}_j + J_2 \sum_{(i,j)_2} \hat{\mathbf{S}}_i \cdot \hat{\mathbf{S}}_j + J_c \sum_{(i,j)_c} \hat{\mathbf{S}}_i \cdot \hat{\mathbf{S}}_j, \quad (1)$$

where J_n and J_c denote the n th-neighbor intralayer and first-neighbor interlayer coupling strengths, respectively [see Fig. 1(b)]. The known magnetic structure of ZVPO dictates that J_c must be negative (i.e., ferromagnetic) and J_2 should be less than $0.4J_1$ [39]. Prior quantitative estimation of the J_1 and J_2 parameters, based on fitting the temperature-dependent magnetization data to high-temperature series expansion (HTSE) predictions, yielded $J_1 = 0.682$ meV and $J_2 = 0.025J_1$ [37]. Also, the isotropy of the spin Hamiltonian [Eq. (1)] is supported by the observation of gapless

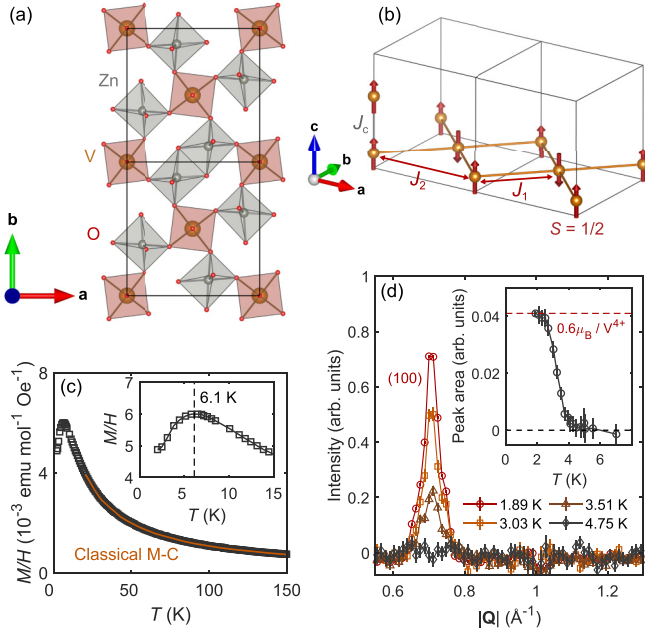


FIG. 1. Structure and magnetic properties of ZVPO. (a) Crystal structure of ZVPO. (b) Magnetic structure of ZVPO [36] and exchange interactions between V^{4+} magnetic moments. (c) Temperature-dependent magnetization of ZVPO under a 1 kOe magnetic field. The inset highlights the position of maximum susceptibility ($T_{\max} = 6.1 \text{ K} = 1.63T_N$). The orange solid line is the magnetic susceptibility obtained from the classical Monte Carlo simulation with the exchange parameters from the high-temperature INS data analysis (Fig. 2). (d) Elastic component ($-0.1 \text{ meV} < E < 0.1 \text{ meV}$) of the neutron scattering data after subtracting the result measured at 10 K, which shows the temperature dependence of the (100) magnetic Bragg peak. The inset shows the peak area fitted by a Gaussian function.

Goldstone modes in ZVPO, even though a tiny Ising-type XXZ anisotropy is anticipated from the spin configuration parallel to the c axis (see the Supplemental Material [22]). Thus, ZVPO can be considered a nearly ideal $S = 1/2$ nearest-neighbor Heisenberg SAFM, as also confirmed by the analysis presented in this work (Fig. 2). The investigation of the spin dynamics in the predominantly classical regime ($T \gg T_N$), when based on the analysis protocol suggested in this work (see the Supplemental Material [22]), allows for credible estimation of the exchange parameters through LLD (Fig. 2). Notably, simultaneous analysis of the energy-resolved excitation spectra measured at various temperatures provides enough information to determine multiple exchange parameters. The optimal values of J_1 , J_2 , and J_c are identified by finding the minimum of the reduced chi square $\chi_r^2(J_1, J_2, J_c)$ between the three measured [Figs. 2(a)–2(c)] and calculated [Figs. 2(a)–2(f)] dynamical susceptibility maps $\chi''(|\mathbf{q}|, E)$ [22]. The agreement between the data and the best fit is exceptional, as evident in the energy-dependent profile of $\chi''(|\mathbf{q}|, E)$ shown in Fig. 2(g).

The minimal χ_r^2 is found for $J_1 = 0.695(15) \text{ meV}$, $J_2 = 0.0(1)J_1$, and $J_c = -0.07(+7, -20)J_1$, with the uncertainties derived from the increase in χ_r^2 of 1. The uncertainty in J_c is asymmetric along its positive and negative directions; thus both values are noted. While these results closely align with the J_1 and J_2 values derived from the HTSE analysis of thermodynamic measurements [37], our analysis indicates more clearly that J_2 is negligible [Figs. 2(h) and 2(i)]. Also, it points towards a more accurate model that incorporates finite J_c (< 0), an essential element for understanding T_N in the $S = 1/2$ SAFM and the ferromagnetic spin configuration along the c axis [Fig. 1(b)]. While the χ_r^2 metric indicates nonzero J_c , its relatively minor impact on the excitation spectra in Figs. 2(a)–2(c) results in a significant uncertainty [Fig. 2(i)]. Nevertheless, the obtained $J_c = -0.07J_1$ is well corroborated

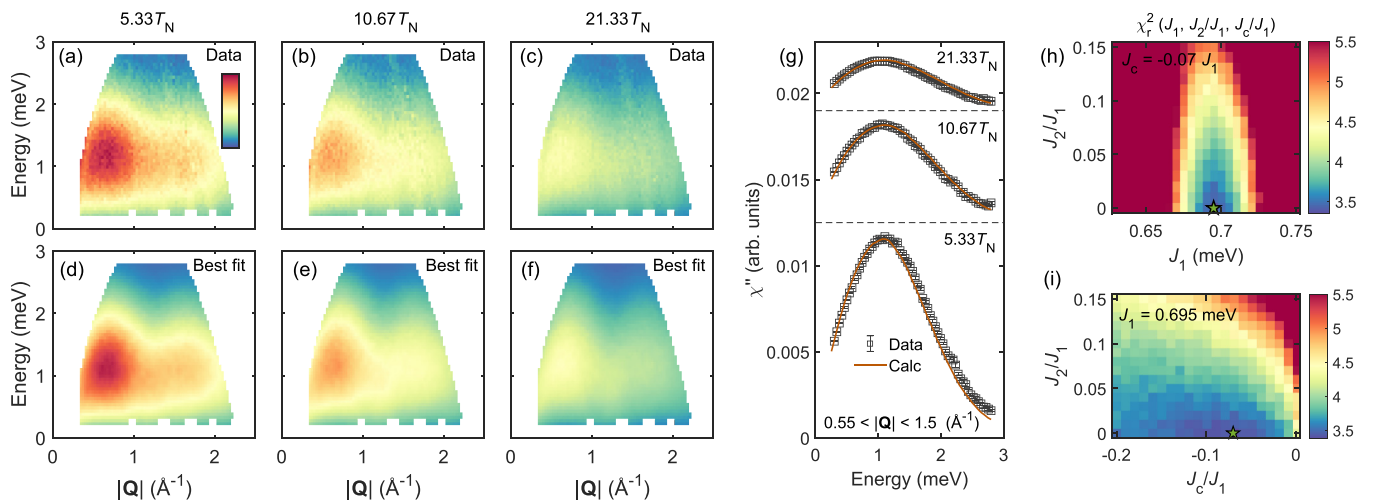


FIG. 2. Spin Hamiltonian obtained by analyzing energy- and momentum-resolved excitation spectra in the classical regime ($T \gg T_N$). (a)–(c) Experimental dynamical susceptibility $\chi''(|\mathbf{q}|, E)$ of ZVPO measured at temperatures above T_N . Background signals in a quasielastic region and near the edge of the detector’s coverage are masked. (d)–(f) Best-fitted $\chi''(|\mathbf{q}|, E)$ to (a)–(c) obtained by LLD. (g) Comparison between the measured and simulated energy dependence of momentum-integrated $\chi''(|\mathbf{q}|, E)$. (h) and (i) Slices of the three-dimensional goodness of fit χ_r^2 (see the Supplemental Material [22]) map around the optimal solution $J_1 = 0.695(15) \text{ meV}$, $J_2 = 0.0(1)J_1$, and $J_c = -0.07(+7, -20)J_1$ plotted as a green star. The uncertainty of the parameters was derived from the increase in χ_r^2 of 1.

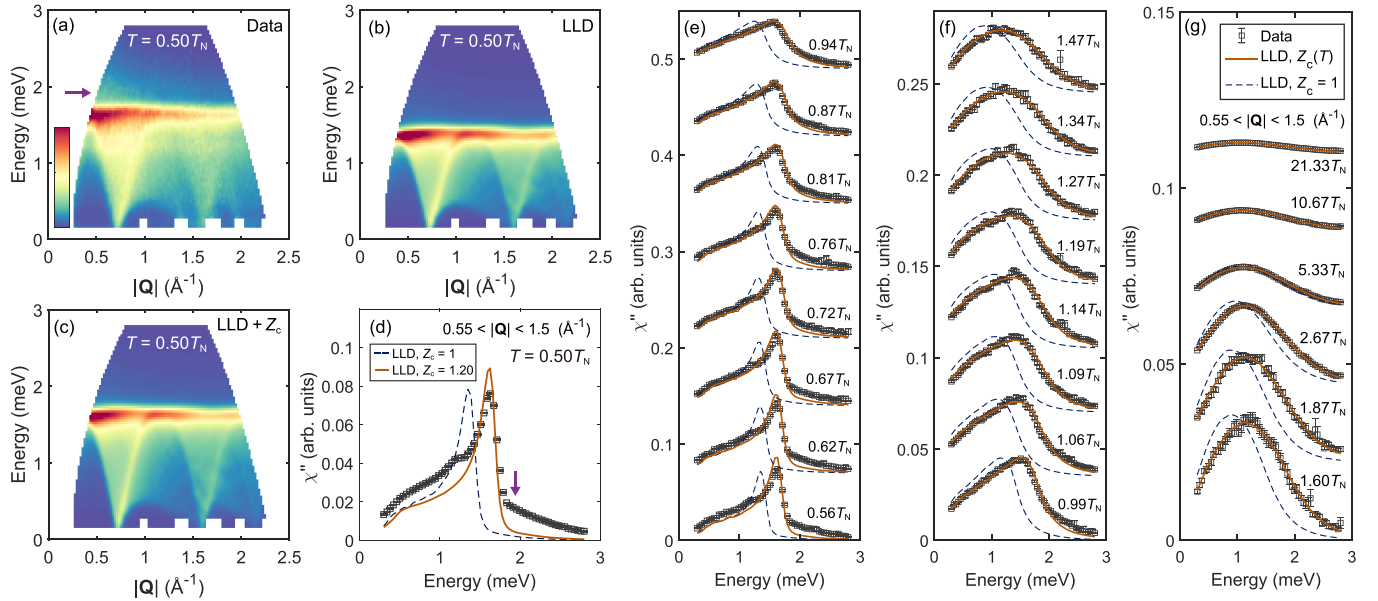


FIG. 3. Comparison between the INS data and the LLD simulations at low temperatures. (a)–(d) Measured and simulated $\chi''(|\mathbf{q}|, E)$ maps at $T = 0.50T_N$. Compared to the LLD result in (b), the result in (c) further involves the quantum renormalization factor $Z_c > 1$, as explained in the text. The low-energy signal observed at around 2 \AA^{-1} in the data originates from acoustic phonons. (e)–(g) Full temperature evolution of the magnetic excitation spectrum plotted via the dynamical susceptibility $\chi''(|\mathbf{q}|, E)$, demonstrating the excellence of the LLD approach in capturing the spin dynamics above T_N and visualizing the transition from quantum to classical spin dynamics. Orange solid (blue dashed) lines are the LLD simulation results with (without) the quantum renormalization factor Z_c .

by our analysis of the $T \ll T_N$ data represented fully by a spin-wave spectrum, which exhibits a unique feature that enables more precise quantification of J_c (see the Supplemental Material [22]). The credibility of the fitted parameters is also evident in the consistency between the measured and calculated temperature dependence of the magnetic susceptibility [Fig. 1(c)], the latter derived from classical Monte Carlo simulations with the spin length normalized to $\sqrt{S(S+1)}$ [22].

Based on the exchange parameters derived in the classical regime ($T \gg T_N$), we extend our analysis to lower temperatures where sizable quantum effects on the spin dynamics are expected. Specifically, we present a comprehensive overview of the temperature effects based on the measured excitation spectra and LLD simulation results at 20 different temperatures ranging from $0.50T_N$ to $2.67T_N$. It is important to emphasize that the simulations are all based on the same exchange parameters obtained from the classical regime at $T \gg T_N$. We initially compare results from the lowest temperature ($T = 0.50T_N$) with minimal thermal fluctuations [see Figs. 3(a), 3(b), and 3(d)]. At such a low temperature, LLD produces nearly the same spin-wave spectrum as LSWT, with both methodologies converging on the same result as the temperature approaches zero [22]. Although the overall shape of the measured spectrum [Fig. 3(a)] resembles the LLD-generated spectrum [Fig. 3(b)], the match in terms of the dynamical susceptibility $\chi''(|\mathbf{q}|, E)$ is not as precise as that found in the classical regime, implying the emergence of quantum effects not captured by the semiclassical LLD approach.

The primary discrepancy at $T = 0.50T_N$ arises from LLD's underestimation of the overall magnon energy scale. This is attributed to the momentum-independent quantum renormalization factor $Z_c > 1$ of the magnon energy $\hbar\omega_{\mathbf{q}}$ in

the Néel-ordered phase of the $S = 1/2$ Heisenberg SAFM [4,32,33],

$$\begin{aligned} \hbar\omega_{\mathbf{q}} &= 2J_1 Z_c \sqrt{\left(1 + \frac{j_c}{2}(1 - \gamma_{\mathbf{q},c})\right)^2 - \gamma_{\mathbf{q},1}^2} \\ &\equiv 2\tilde{J}_1 \sqrt{\left(1 + \frac{j_c}{2}(1 - \gamma_{\mathbf{q},c})\right)^2 - \gamma_{\mathbf{q},1}^2}, \end{aligned} \quad (2)$$

where $j_c = |J_c|/J_1$ (with $J_1 > 0$ and $J_c < 0$), while $\gamma_{\mathbf{q},1} = \frac{1}{4} \sum_{\delta_1} \cos(\mathbf{q} \cdot \delta_1)$ and $\gamma_{\mathbf{q},c} = \frac{1}{2} \sum_{\delta_c} \cos(\mathbf{q} \cdot \delta_c)$ in terms of the intralayer and interlayer bond vectors δ_1 and δ_c . Typically, Z_c is incorporated into J_1 by defining an effective coupling strength \tilde{J}_1 , as in the second line of Eq. (2). This is because analyzing the spin-wave spectrum only reveals the value of $\tilde{J}_1 = Z_c J_1$, leaving J_1 itself ambiguous unless the theoretical value of Z_c is utilized [29]. However, by first analyzing the classical regime $T \gg T_N$ (Fig. 2), our methodology enables direct access to J_1 as the influence of Z_c vanishes at sufficiently high temperatures. Consequently, the magnitude of Z_c can be explicitly visualized through a comparison between the data [Fig. 3(a)] and the LLD simulations [Fig. 3(b)].

Moreover, assuming that J_1 is independent of temperature (which is mostly true unless a system undergoes a structural phase transition), Z_c can be experimentally quantified by matching the energy scale of the LLD simulation to the observed spin-wave spectrum. For instance, as shown in Fig. 3(d), $\tilde{J}_1 \sim 1.2J_1$ best describes the magnon energies measured at $T = 0.5T_N$. Importantly, this value is consistent with the theoretical result $Z_c = 1.18(2)$ at zero temperature, predicted by spin-wave theory up to the order of $1/S^2$ [31] or the series expansion technique [30]. This validates the

high precision of the exchange parameters derived from our refinement process in the classical regime (Fig. 2).

Another apparent discrepancy between the data and the LLD simulation result is the continuum scattering we observe above the one-magnon spectrum ($E > 1.8$ meV), as indicated by purple arrows in Figs. 3(a) and 3(d). Notably, according to Fig. 3(d), the spectral weight of this continuum scattering is approximately 17% of that from the one-magnon modes. This continuum is likely a combination of two-magnon scattering that becomes most significant at $\mathbf{q} = (\pi, \pi)$ [$|\mathbf{Q}| = 0.71$ Å in Fig. 3(a)] [4,32,33] and fractionalized quasiparticles that dominate the spectrum around $\mathbf{q} = (\pi, 0)$ [$|\mathbf{Q}| = 0.50$ or 1.12 Å in Fig. 3(a)] [8,9]. A comparison between the observed continuum signal and the theoretical dynamical structure factor of the two-magnon continuum is presented in the Supplemental Material [22].

Expanding the analysis to higher temperatures ($T > 0.5T_N$) yields a complete temperature-dependent profile of $Z_c(T)$ and the continuum scattering. Figures 3(e)–3(g) show the measured energy dependence of $\chi''(|\mathbf{q}|, E)$, with $|\mathbf{q}|$ integrated from 0.55 Å⁻¹ to 1.5 Å⁻¹, and the corresponding LLD simulations with (orange solid lines) and without (blue dashed lines) the best-fitted $Z_c(T)$ for each temperature. We again emphasize that the calculations in Figs. 3(e)–3(g) are all based on the same set of exchange parameters. The dashed lines are derived by applying an individual multiplicative scaling factor of χ'' for each temperature, whereas the solid lines are obtained by fitting both the multiplicative scaling factor and the Z_c parameter for each temperature. For selected temperatures, a detailed comparison of the energy- and momentum-resolved spectra is available in the Supplemental Material [22]. As long as the excitation energies are appropriately rescaled by the temperature-dependent but momentum-independent $Z_c(T)$, good agreement is found for temperatures down to about $1.1T_N$ [Figs. 3(f) and 3(g)]. This illustrates LLD's capability to model the spin dynamics of the $S = 1/2$ Heisenberg SAFM above T_N .

The resultant $Z_c(T)$ is shown in Fig. 4(a). As expected, $Z_c(T)$ converges towards 1.18 for $T \ll T_N$ and approaches 1 in the high-temperature regime $T \gg T_N$. Interestingly, however, the behavior of $Z_c(T)$ in the intermediate-temperature range defies a simple monotonic progression from $Z_c(T = 0) = 1.18$ to $Z_c(T \gg T_N) = 1$. Instead, $Z_c(T)$ gradually increases as T approaches T_N and reaches its maximum between T_N and the temperature of maximum susceptibility $T_{\max} \sim 1.6T_N$, similar to the trend observed in the temperature-dependent magnetization [Fig. 1(c)]. Nevertheless, we caution against overinterpreting this finding due to one limitation of our current LLD model: It relies on Boltzmann statistics to model thermal fluctuations, which likely results in an overestimation of thermal fluctuations around T_N [17]. Such an overestimation becomes apparent when comparing the measured and calculated intensities of the magnetic (100) peak [Fig. 4(c)], the latter of which was obtained from LLD simulations. As this would lead to the underestimation of excitation energies around $T = T_N$, the unusual behavior of $Z_c(T)$ near T_N may blend the actual quantum renormalization effect with adjustments for overestimated thermal fluctuations. Thus, accessing the true nature of $Z_c(T)$ around T_N first requires disentangling these two factors, which we leave as

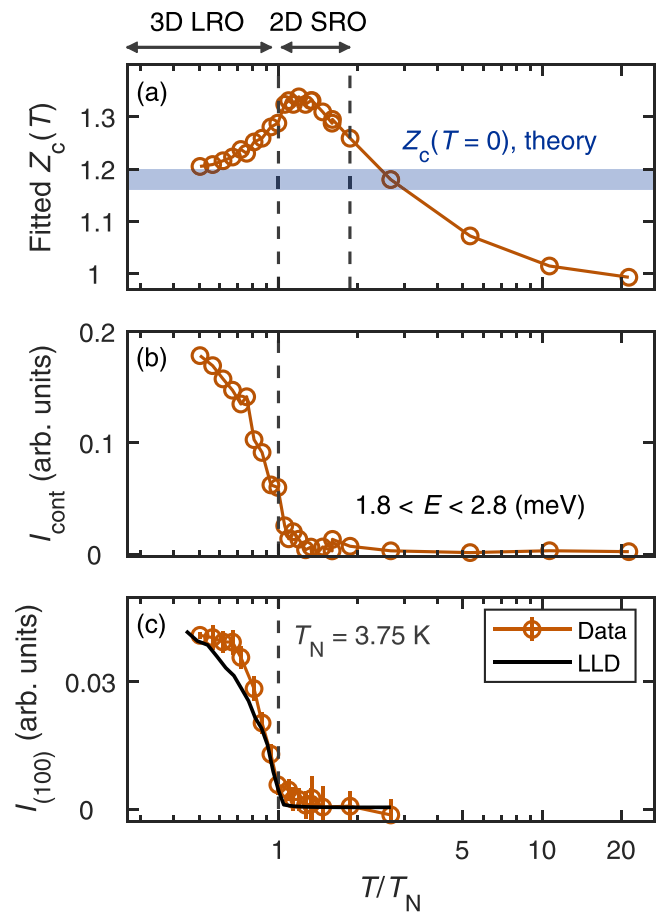


FIG. 4. Temperature dependence of the quantum effects in the spin dynamics of ZVPO. (a) Temperature-dependent quantum renormalization factor $Z_c(T)$, obtained by dividing the optimal $\tilde{J}_1(T)$ at each temperature with $J_1 = 0.695$ meV. Two arrows on the top indicate the ranges with 3D long-range order (LRO) and 2D short-range order (SRO) [36]. (b) Temperature-dependent intensity of the quantum continuum I_{cont} , obtained by integrating the remnant intensities underestimated by LLD [orange solid lines in Figs. 3(e)–3(g)] above 1.8 meV. (c) Temperature-dependent intensity of the (100) magnetic Bragg peak. The data (open circles) are the same as the inset of Fig. 1(d). Note that the reduced temperature T/T_N is plotted in logarithmic scale for better presentation.

a future challenge. It can be potentially achieved by refining the current LLD approach to better follow the Bose-Einstein statistics, as suggested in Refs. [17,40].

Analyzing the temperature dependence of the continuum scattering also reveals important insights. First of all, it is crucial to recognize that thermal fluctuations already induce a continuumlike signal above the one-magnon bands at sufficiently high temperatures (referred to as a thermal continuum), as evident from the LLD simulation results shown in Figs. 3(e) and 3(f). Thus, the quantum continuum, resulting from two-magnon scattering and fractionalized quasiparticles, must be distinguished by isolating the spectral weight not captured by the semiclassical LLD simulations. Indeed, LLD consistently underestimates $\chi''(|\mathbf{q}|, E)$ above the one-magnon band ($E > 1.8$ meV) for T below approximately $1.1T_N$ [see Figs. 3(d)–3(f)]. Figure 4(b) shows the integral of

underestimated $\chi''(|\mathbf{q}|, E)$ above 1.8 meV at each temperature, exhibiting a similar trend to the magnetic Bragg peak intensity [Fig. 4(c)]. In other words, the emergence of the quantum continuum is marginal above T_N , implying its relevance to the formation of 3D long-range order. Conversely, the regime characterized by 2D short-range correlations (around T_{\max}) is still well described by semiclassical LLD simulations. For completeness, however, additional examination using $S = 1/2$ SAFMs with significantly weaker J_c (e.g., cuprates [29]) is required since the observed temperature dependence might have been affected by the non-negligible strength of J_c in ZVPO (5–7% of J_1).

The comparative analysis of temperature dependence presented in this study demonstrates the proficiency of LLD in both accurately determining the spin Hamiltonian of quantum antiferromagnets and visualizing the quantum-to-classical crossover in their spin dynamics. Specifically, the remarkable agreement between the experimental data and the LLD simulations above T_N encourages the extension of this approach to more challenging $S = 1/2$ systems with much stronger quantum fluctuations, in which the excitation spectra below T_N are expected to have larger deviations from predictions based on conventional spin-wave theory. Low-dimensional frustrated magnets, such as the $S = 1/2$ triangular lattice antiferromagnet [2,10] or the $S = 1/2$ honeycomb antiferromagnet proximate to the suggested Kitaev spin liquid phase [12], stand out as promising examples, as also suggested in another recent theoretical study [41].

The successful application of the LLD approach to powder-averaged data merits further discussion regarding both its implications and potential challenges. The extraction of optimal exchange parameters consistent with previous studies and the quantitative determination of $Z_c(T = 0) = 1.19$, as previously calculated by theory, indicates that our

LLD approach can be useful even for powder-averaged data. This capability not only broadens the scope of materials that can be explored experimentally but also allows the spectroscopic study of quantum antiferromagnets to proceed more rapidly. However, it is important to interpret the analysis results of powder-averaged spectra with caution. The analysis is typically challenged by the significant loss of information due to powder averaging, which can lead to considerable parameter uncertainty from the fitting or even potential nonunique solutions. Thus, a rigorous evaluation of the fitting results, such as the standard statistical analysis of parameters' uncertainties using reduced χ^2 and exploring the χ^2 map around the solution [Figs. 2(h) and 2(i)], is essential. Also, the approach described here is not restricted to measurements of polycrystalline samples; it can also be readily applied to single-crystal studies. This will reveal deeper physical insights not evident in a powder-averaged spectrum, such as momentum-dependent magnon decay and/or renormalization. The LLD calculation protocol suggested in this work [22] can be directly applied to such future efforts. Overall, our findings highlight the potential of LLD in exploring the dynamics of systems at the forefront of quantum magnetism research.

We acknowledge C. Batista for fruitful discussions about the LLD approach and its results. This research was supported by the U.S. Department of Energy, Office of Science, Basic Energy Sciences, Materials Science and Engineering Division. A portion of this research used resources at the Spallation Neutron Source, a DOE Office of Science User Facility operated by the Oak Ridge National Laboratory. Sample synthesis was supported by the Laboratory Directed Research and Development Program of Oak Ridge National Laboratory, managed by UT-Battelle, LLC, for the U.S. Department of Energy.

-
- [1] J. Ma, Y. Kamiya, T. Hong, H. B. Cao, G. Ehlers, W. Tian, C. D. Batista, Z. L. Dun, H. D. Zhou, and M. Matsuda, Static and dynamical properties of the spin-1/2 equilateral triangular-lattice antiferromagnet $\text{Ba}_3\text{CoSb}_2\text{O}_9$, *Phys. Rev. Lett.* **116**, 087201 (2016).
- [2] S. Ito, N. Kurita, H. Tanaka, S. Ohira-Kawamura, K. Nakajima, S. Itoh, K. Kuwahara, and K. Kakurai, Structure of the magnetic excitations in the spin-1/2 triangular-lattice Heisenberg antiferromagnet $\text{Ba}_3\text{CoSb}_2\text{O}_9$, *Nat. Commun.* **8**, 235 (2017).
- [3] D. Macdougall, S. Williams, D. Prabhakaran, R. I. Bewley, D. J. Voneshen, and R. Coldea, Avoided quasiparticle decay and enhanced excitation continuum in the spin- $\frac{1}{2}$ near-Heisenberg triangular antiferromagnet $\text{Ba}_3\text{CoSb}_2\text{O}_9$, *Phys. Rev. B* **102**, 064421 (2020).
- [4] J. Lorenzana, G. Seibold, and R. Coldea, Sum rules and missing spectral weight in magnetic neutron scattering in the cuprates, *Phys. Rev. B* **72**, 224511 (2005).
- [5] G. Sala, M. B. Stone, B. K. Rai, A. F. May, P. Laurell, V. O. Garlea, N. P. Butch, M. D. Lumsden, G. Ehlers, G. Pokharel *et al.*, Van Hove singularity in the magnon spectrum of the antiferromagnetic quantum honeycomb lattice, *Nat. Commun.* **12**, 171 (2021).
- [6] C. Kim, S. Kim, P. Park, T. Kim, J. Jeong, S. Ohira-Kawamura, N. Murai, K. Nakajima, A. Chernyshev, M. Mourigal *et al.*, Bond-dependent anisotropy and magnon decay in cobalt-based Kitaev triangular antiferromagnet, *Nat. Phys.* **19**, 1624 (2023).
- [7] G. Sala, M. B. Stone, G. B. Halász, M. D. Lumsden, A. F. May, D. M. Pajerowski, S. Ohira-Kawamura, K. Kaneko, D. G. Mazzone, G. Simutis, J. Lass, Y. Kato, S.-H. Do, J. Y. Y. Lin, and A. D. Christianson, Field-tuned quantum renormalization of spin dynamics in the honeycomb lattice Heisenberg antiferromagnet YbCl_3 , *Commun. Phys.* **6**, 234 (2023).
- [8] B. Dalla Piazza, M. Mourigal, N. B. Christensen, G. J. Nilsen, P. Tregenna-Piggott, T. G. Perring, M. Enderle, D. F. McMorrow, D. A. Ivanov, and H. M. Rønnow, Fractional excitations in the square-lattice quantum antiferromagnet, *Nat. Phys.* **11**, 62 (2015).
- [9] N. B. Christensen, H. M. Rønnow, D. F. McMorrow, A. Harrison, T. G. Perring, M. Enderle, R. Coldea, L. P. Regnault, and G. Aeppli, Quantum dynamics and entanglement of spins on a square lattice, *Proc. Natl. Acad. Sci. USA* **104**, 15264 (2007).
- [10] A. Scheie, E. Ghioldi, J. Xing, J. Paddison, N. Sherman, M. Dupont, L. Sanjeeva, S. Lee, A. Woods, D. Abernathy *et al.*,

- Proximate spin liquid and fractionalization in the triangular antiferromagnet KYbSe₂, *Nat. Phys.* **20**, 74 (2024).
- [11] P. Park, E. Ghioldi, A. F. May, J. A. Kolopus, A. A. Podlesnyak, J. A. Paddison, C. D. Batista, A. Trumper, L. Manuel, M. B. Stone *et al.*, Anomalous continuum scattering and higher-order van Hove singularity in the strongly anisotropic $S = 1/2$ triangular lattice antiferromagnet, [arXiv:2403.03210](https://arxiv.org/abs/2403.03210).
- [12] A. Banerjee, J. Yan, J. Knolle, C. A. Bridges, M. B. Stone, M. D. Lumsden, D. G. Mandrus, D. A. Tennant, R. Moessner, and S. E. Nagler, Neutron scattering in the proximate quantum spin liquid α -RuCl₃, *Science* **356**, 1055 (2017).
- [13] T. Xie, A. Eberharter, J. Xing, S. Nishimoto, M. Brando, P. Khanenko, J. Sichelschmidt, A. Turrini, D. Mazzone, P. Naumov *et al.*, Complete field-induced spectral response of the spin-1/2 triangular-lattice antiferromagnet CsYbSe₂, *npj Quantum Mater.* **8**, 48 (2023).
- [14] E. A. Ghioldi, S.-S. Zhang, Y. Kamiya, L. O. Manuel, A. E. Trumper, and C. D. Batista, Evidence of two-spinon bound states in the magnetic spectrum of Ba₃CoSb₂O₉, *Phys. Rev. B* **106**, 064418 (2022).
- [15] Y. Kamiya, L. Ge, T. Hong, Y. Qiu, D. Quintero-Castro, Z. Lu, H. Cao, M. Matsuda, E. Choi, C. Batista *et al.*, The nature of spin excitations in the one-third magnetization plateau phase of Ba₃CoSb₂O₉, *Nat. Commun.* **9**, 2666 (2018).
- [16] A. O. Scheie, Y. Kamiya, H. Zhang, S. Lee, A. J. Woods, M. O. Ajeesh, M. G. Gonzalez, B. Bernu, J. W. Villanova, J. Xing, Q. Huang, Q. Zhang, J. Ma, E. S. Choi, D. M. Pajerowski, H. Zhou, A. S. Sefat, S. Okamoto, T. Berlijn, L. Messio *et al.*, Nonlinear magnons and exchange Hamiltonians of the delafossite proximate quantum spin liquid candidates KYbSe₂ and NaYbSe₂, *Phys. Rev. B* **109**, 014425 (2024).
- [17] D. Dahlbom, F. T. Brooks, M. S. Wilson, S. Chi, A. I. Kolesnikov, M. B. Stone, H. Cao, Y.-W. Li, K. Barros, M. Mourigal, C. D. Batista, and X. Bai, Quantum-to-classical crossover in generalized spin systems: Temperature-dependent spin dynamics of FeI₂, *Phys. Rev. B* **109**, 014427 (2024).
- [18] J. A. M. Paddison, B. K. Rai, A. F. May, S. Calder, M. B. Stone, M. D. Frontzek, and A. D. Christianson, Magnetic interactions of the centrosymmetric skyrmion material Gd₂PdSi₃, *Phys. Rev. Lett.* **129**, 137202 (2022).
- [19] J. A. M. Paddison, Scattering signatures of bond-dependent magnetic interactions, *Phys. Rev. Lett.* **125**, 247202 (2020).
- [20] D. Dahlbom, H. Zhang, C. Miles, X. Bai, C. D. Batista, and K. Barros, Geometric integration of classical spin dynamics via a mean-field Schrödinger equation, *Phys. Rev. B* **106**, 054423 (2022).
- [21] D. Dahlbom, C. Miles, H. Zhang, C. D. Batista, and K. Barros, Langevin dynamics of generalized spins as SU(N) coherent states, *Phys. Rev. B* **106**, 235154 (2022).
- [22] See Supplemental Material at <http://link.aps.org/supplemental/10.1103/PhysRevResearch.6.033184> for explanations of the sample preparation, the detailed procedure of calculating dynamical susceptibility at finite temperatures, the classical Monte Carlo simulation, the optimization of exchange parameters, the presence of gapless goldstone modes, the more precise estimation of J_c , the calculation of a two-magnon continuum, and energy- and momentum-resolved spectra between $0.5T_N$ and $10.67T_N$. It also contains Refs. [23,24].
- [23] S. Zhang, H. J. Changlani, K. W. Plumb, O. Tchernyshyov, and R. Moessner, Dynamical structure factor of the three-dimensional quantum spin liquid candidate NaCaNi₂F₇, *Phys. Rev. Lett.* **122**, 167203 (2019).
- [24] T. Proffen and T. Welberry, Analysis of diffuse scattering via the reverse Monte Carlo technique: A systematic investigation, *Acta Crystallogr. A* **53**, 202 (1997).
- [25] T. Huberman, D. Tennant, R. Cowley, R. Coldea, and C. Frost, A study of the quantum classical crossover in the spin dynamics of the 2D $S = 5/2$ antiferromagnet Rb₂MnF₄: Neutron scattering, computer simulations and analytic theories, *J. Stat. Mech.* (2008) P05017.
- [26] X. Bai, J. A. M. Paddison, E. Kapit, S. M. Koohpayeh, J.-J. Wen, S. E. Dutton, A. T. Savici, A. I. Kolesnikov, G. E. Granroth, C. L. Broholm, J. T. Chalker, and M. Mourigal, Magnetic excitations of the classical spin liquid MgCr₂O₄, *Phys. Rev. Lett.* **122**, 097201 (2019).
- [27] A. Auerbach and D. P. Arovas, Spin dynamics in the square-lattice antiferromagnet, *Phys. Rev. Lett.* **61**, 617 (1988).
- [28] K. Yamada, K. Kakurai, Y. Endoh, T. R. Thurston, M. A. Kastner, R. J. Birgeneau, G. Shirane, Y. Hidaka, and T. Murakami, Spin dynamics in the two-dimensional quantum antiferromagnet La₂CuO₄, *Phys. Rev. B* **40**, 4557 (1989).
- [29] R. Coldea, S. M. Hayden, G. Aeppli, T. G. Perring, C. D. Frost, T. E. Mason, S.-W. Cheong, and Z. Fisk, Spin waves and electronic interactions in La₂CuO₄, *Phys. Rev. Lett.* **86**, 5377 (2001).
- [30] R. R. P. Singh, Thermodynamic parameters of the $T = 0$, spin-1/2 square-lattice Heisenberg antiferromagnet, *Phys. Rev. B* **39**, 9760 (1989).
- [31] C. M. Canali, S. M. Girvin, and M. Wallin, Spin-wave velocity renormalization in the two-dimensional Heisenberg antiferromagnet at zero temperature, *Phys. Rev. B* **45**, 10131 (1992).
- [32] T. Huberman, R. Coldea, R. A. Cowley, D. A. Tennant, R. L. Leheny, R. J. Christianson, and C. D. Frost, Two-magnon excitations observed by neutron scattering in the two-dimensional spin- $\frac{5}{2}$ Heisenberg antiferromagnet Rb₂MnF₄, *Phys. Rev. B* **72**, 014413 (2005).
- [33] A. N. Petsch, N. S. Headings, D. Prabhakaran, A. I. Kolesnikov, C. D. Frost, A. T. Boothroyd, R. Coldea, and S. M. Hayden, High-energy spin waves in the spin-1 square-lattice antiferromagnet La₂NiO₄, *Phys. Rev. Res.* **5**, 033113 (2023).
- [34] Su(n)ny, Spin dynamics and generalization to SU(N) coherent states, <https://github.com/sunnysuite/sunny.jl>.
- [35] O. Arnold, J.-C. Bilheux, J. Borreguero, A. Buts, S. I. Campbell, L. Chapon, M. Doucet, N. Draper, R. F. Leal, M. Gigg *et al.*, Mantid—Data analysis and visualization package for neutron scattering and μ SR experiments, *Nucl. Instrum. Methods Phys. Res. Sect. A* **764**, 156 (2014).
- [36] S. M. Yusuf, A. K. Bera, N. S. Kini, I. Mirebeau, and S. Petit, Two- and three-dimensional magnetic correlations in the spin- $\frac{1}{2}$ square-lattice system Zn₂VO(PO₄)₂, *Phys. Rev. B* **82**, 094412 (2010).
- [37] N. Kini, E. Kaul, and C. Geibel, Zn₂VO(PO₄)₂: An $S = 1/2$ Heisenberg antiferromagnetic square lattice system, *J. Phys.: Condens. Matter* **18**, 1303 (2006).

- [38] A. Yogi, N. Ahmed, R. Nath, A. A. Tsirlin, S. Kundu, A. V. Mahajan, J. Sichelschmidt, B. Roy, and Y. Furukawa, Antiferromagnetism of $\text{Zn}_2\text{VO}(\text{PO}_4)_2$ and the dilution with Ti^{4+} , *Phys. Rev. B* **91**, 024413 (2015).
- [39] H.-C. Jiang, H. Yao, and L. Balents, Spin liquid ground state of the spin- $\frac{1}{2}$ square J_1 - J_2 Heisenberg model, *Phys. Rev. B* **86**, 024424 (2012).
- [40] A. V. Savin, Y. A. Kosevich, and A. Cantarero, Semiquantum molecular dynamics simulation of thermal properties and heat transport in low-dimensional nanostructures, *Phys. Rev. B* **86**, 064305 (2012).
- [41] A. M. Samarakoon, A. Banerjee, S.-S. Zhang, Y. Kamiya, S. E. Nagler, D. A. Tennant, S.-H. Lee, and C. D. Batista, Comprehensive study of the dynamics of a classical Kitaev spin liquid, *Phys. Rev. B* **96**, 134408 (2017).